Detection of SF_6 decomposition gases by the pristine and Fe-doped porphyrin based on the first-principles calculations

Xing He[1], Enrui Dai[1*], Rou Xue[1], Qiaowen Chang[2], Huihui Xiong[3] and Zhifeng Nie[1*]

[1] Yunnan Key Laboratory of Metal-Organic Molecular Materials and Device, School of Chemistry and Chemical Engineering, Kunming University, Kunming 650214, China.
[2] Kunming Institute of Precious Metals, Yunnan Precious Metals Lab., LTD, Kunming 650106, China
[3] School of Metallurgy Engineering, Jiangxi University of Science and Technology, Ganzhou 34100, China
* Correspondence: daienr@163.com, niezf123@163.com.

Abstract: The development of high-performance sensing materials for detecting or removing SF_6 decomposition gases is crucial for gas-insulated switchgear (GIS). In this work, the adsorption characteristics of the pristine porphyrin (Pr) and Fe-doped porphyrin (FePr) monolayers towards SF_6 decomposition gases were investigated using the first-principles calculations. Additionally, the electronic properties and sensing-mechanism were also examined. The findings indicate that both Pr and FePr monolayers exhibit thermodynamic stability. The intrinsic Pr monolayer only exhibits a moderate affinity towards the SO_2 molecule, however, its poor sensitivity of the Pr monolayer renders it unsuitable as the sensing-material. In contrast, the FePr monolayer exhibits favorable adsorption strength towards all five toxic gases (H_2S, SO_2, SOF_2, SO_2F_2, HF). The FePr monolayer exhibits chemisorption towards SO_2/SOF_2 gases, Furthermore, the microscopic mechanism of gases-substrate interaction is elucidated through the analysis of charge density difference, charge transfer, and density of states. Moreover, the FePr has excellent sensitivity for H_2S, SO_2, SO_2F_2, SOF_2 and HF molecules owing to the significant variations of the band gap, electrical conductivity and work function. In addition, the τ of H_2S, SO_2, and SOF_2 is 12.6 μs, 18.5 s and 15.4 s at 298 K, respectively. Our calculated results can offer theoretical guidance for the practical application of FePr-based sensing materials to detect SF_6 decompositions gases.

Keywords: FePr monolayer; SF_6 decomposition gases; First-principles calculations; Sensing mechanism

1. Introduction

Sulfur hexafluoride (SF_6) is a colorless gas that is primarily non-toxic and non-flammable [1, 2]. Due to its high electronegativity, exceptional arc extinguishing properties, superior insulation strength and excellent thermal conductivity, SF_6 is widely employed as a dielectric gas in gas-insulated switchgear (GIS) [3-6]. However, the prolonged operation of gas-insulated equipment inevitably leads to the occurrence of partial discharges (PD), resulting in the decomposition of SF_6 into some toxic gases such as H_2S, SO_2, SOF_2, SO_2F_2 and HF through reactions with oxygen and water vapor [7-9]. If these gases are not promptly detected or removed, they may accelerate the deterioration of gas equipment insulation and contribute to air pollution [10, 11]. Therefore, it is crucial to detect or eliminate the release of SF_6 decomposition component gases from both environmental and health perspectives [12]. This can be accomplished by developing a gas sensing material that exhibits superior performance.

The potential of two-dimensional (2D) materials as adsorbent materials for environmental protection is significant due to their high surface area, controlled interlayer bonding, specific binding capacity, chemical stability and sensitivity [13, 14]. In recent years, a variety of 2D materials, including 2D sulfur compounds [2, 15], ZnO [16], C_3N [17], MXenes [18], graphene [19]

* Corresponding author.
E-mail address: daienr@163.com, niezf123@163.com

Preprints (www.preprints.org) | NOT PEER-REVIEWED | Posted: 13 June 2023 doi:10.20944/preprints202306.0912.v1

and the group III–V nitrides [20] have demonstrated high efficacy in the detecting and capturing harmful gases. For instance, Hu et al. [21] investigated the adsorption characteristics of NH_3, CO and NO_2 on SnS monolayers, and the results showed that there exists a significant adsorption effect of NO_2 on the SnS monolayers. To fully exploit the potential of transition metal-doped InN monolayers as sensors for toxic gases, Guo et al. [22] proposed the utilization of InN monolayers decorated with Pd, Pt, Ag, and Au for NO_2 sensing applications. However, they are always plagued by issues of structural instability, limited lifespan, high cost, and susceptibility to external interference, which ultimately restricts the research and application of gas sensors.

Recently, it has become widely recognized that organic macromolecule porphyrins possess significant electron-donating properties due to their abundant p electrons and extended π-bonds. The intrinsic advantages have facilitated the utilization of porphyrins in advanced technological applications, encompassing spintronics, electrocatalysis, and gas sensors [23-27]. For instance, Wang et al. [28] investigated the sensing properties of 2D metal-porphyrin porous nanosheets towards CO, NO, NO_2 gases, the results indicated that the FePP-Grid and ZnPP-Grid could be used for the detection of CO, NO and NO_2. The redox properties of 2D iron porphyrin nanosheets were investigated through DFT calculations by Luo et al., revealing their electronic structure and potential applications in catalysis [29]. According to previous reports [30], the transition metal (TM) atom in 2D metalloporphyrin molecules exhibits exceptional catalytic activity due to charge transfer between reactant molecules and TM. Therefore, the central TM atom may function as an active site for capturing or detecting SF_6 decomposition gases.

In this study, we conducted a first-principles study to investigate the sensing properties of five major gases (H_2S, SO_2, SOF_2, SO_2F_2, and HF) on the intrinsic porphyrin (Pr) and Fe-doped porphyrin (FePr) monolayers. Firstly, the thermal stability of FePr was verified, followed by a comprehensive analysis of the adsorption energies and electronic properties across various adsorption systems. Furthermore, the gas sensing efficacy of FePr towards five main SF_6 decomposition components was assessed by analyzing the variation in band gap and work function. Finally, the magnetic properties and recovery times of a FePr monolayer were examined to assess its suitability for sensing applications in adsorbing or detecting SF_6 decomposition gases.

2. Computational methods

All the spin calculations were conducted using the DMol^3 package [31] within Materials Studio software, employing the density functional theory (DFT) method. The Perdew-Burke-Ernzerhof (PBE) function under the generalized gradient approximation (GGA) was selected to describe electron-electron interaction [32]. To ensure the precision of calculation results, we employed the DFT-D method proposed by Grimme [33] to correct the interactions between gases and FePr. The DNP basis set with a cutoff radius of 5.2 Å [34] and the DFT semi-core pseudopotential (DSSP) [35] method were employed in the simulation process. For structure optimization and electronic structure calculation, a k-point mesh with dimensions of 5×5×1 was employed [36]. The selection of a vacuum layer with a thickness of 20 Å in the z-direction effectively prevents interactions between adjacent units [37]. The energy tolerance accuracy was set to 1.0×10^{-5} Ha, while the maximum force and convergence displacement tolerances were set to 0.002 Ha/Å and 0.005 Å, respectively.

To assess the adsorption strength of gas molecules on the substrate, we calculated the adsorption energy (E_{ads}) using the following equation [38]:

$$E_{ads} = E_{gas+substrate} - E_{substrate} - E_{gas} \quad (1)$$

Where $E_{gas+substrate}$ represents the total energy of the gas adsorbed on the substrate, with $E_{substrate}$ and E_{gas} denoting the energies of the substrate and gas, respectively. If the absolute value of adsorption energy is greater than 0.5 eV, the adsorption process can be classified as chemical adsorption, otherwise, it is considered to be physical adsorption [39]. Moreover, the charge transfer from the FePr monolayer to a gas molecule can be calculated based on Mulliken charges by using the following equation [40]:

$$Q_T = Q_{adsorbed\ molecule} - Q_{isolated\ molecule} \quad (2)$$

Preprints (www.preprints.org) | NOT PEER-REVIEWED | Posted: 13 June 2023 doi:10.20944/preprints202306.0912.v1

where $Q_{\text{adsorbed molecule}}$ and $Q_{\text{isolated molecule}}$ denote the number of charges of before and after adsorption, respectively. When $Q_T > 0$, it signifies that the gas molecule donates its electrons to the FePr monolayer, with the gas molecule acting as an electron donor. Moreover, the CDD of various adsorption systems can be computed using the following equation [41]:

$$\Delta\rho = \rho_{\text{FePr/gas}} - (\rho_{\text{FePr}} + \rho_{\text{gas}}) \quad (3)$$

Where $\rho_{\text{FePr/gas}}$, ρ_{FePr}, and ρ_{gas} represent the charge density of a gas-adsorbed FePr monolayer, FePr monolayer and single gas molecules, respectively.

3. Results and discussion

3.1. Structural and electronic properties of Pr monolayer and FePr monolayer

Fig. 1(a) displays the FePr monolayer consisting of 24 carbon (C) atoms, four nitrogen (N) atoms, eight hydrogen (H) atoms, and one transition metal iron (Fe) atom. When Fe atom is introduced into the Pr monolayer, all atoms are coplanar. The calculated lattice parameter of 10.85Å exhibits excellent conformity with other experimentally determined values [42]. Different adsorption styles of gas molecules were taken into account when the SF_6 decomposition gases approached the surface of FePr in Fig. 1(b). For example, the adsorption of SO_2 molecule on FePr monolayer exhibits two distinct patterns, namely S-end and O-end, with S atoms and O atoms oriented, respectively. The definition method was also employed for the remaining molecules investigated in this work.

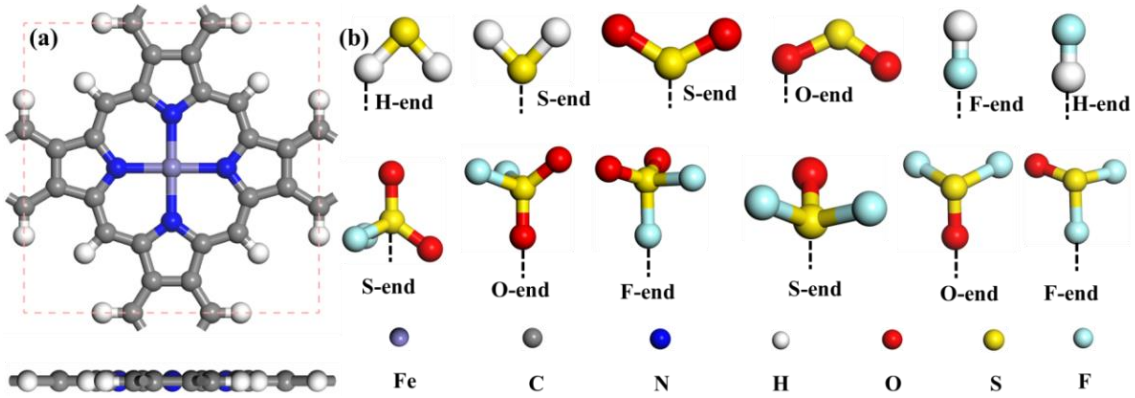

Figure 1. (a) The configuration of top views and side views of the FePr monolayer and (b) the adsorption configurations of the different gases on FePr monolayer.

The binding energy of the FePr monolayer, as presented in Fig. 2(a), is observed to be lower than that of bulk Fe. The result indicates that the FePr monolayer exhibits exceptional thermodynamic stability [43]. As depicted in Fig.2 (a-b), the intrinsic Pr and FePr monolayers exhibit semi-metallic characteristics due to their zero band gap. It is noteworthy that the introduction of the Fe atom into pristine Pr results in the emergence of magnetic properties in the FePr monolayer. Specifically, the spin-down bands intersect with the Fermi energy level while the spin-up bands are situated at a considerable distance from it.

Preprints (www.preprints.org) | NOT PEER-REVIEWED | Posted: 13 June 2023 doi:10.20944/preprints202306.0912.v1

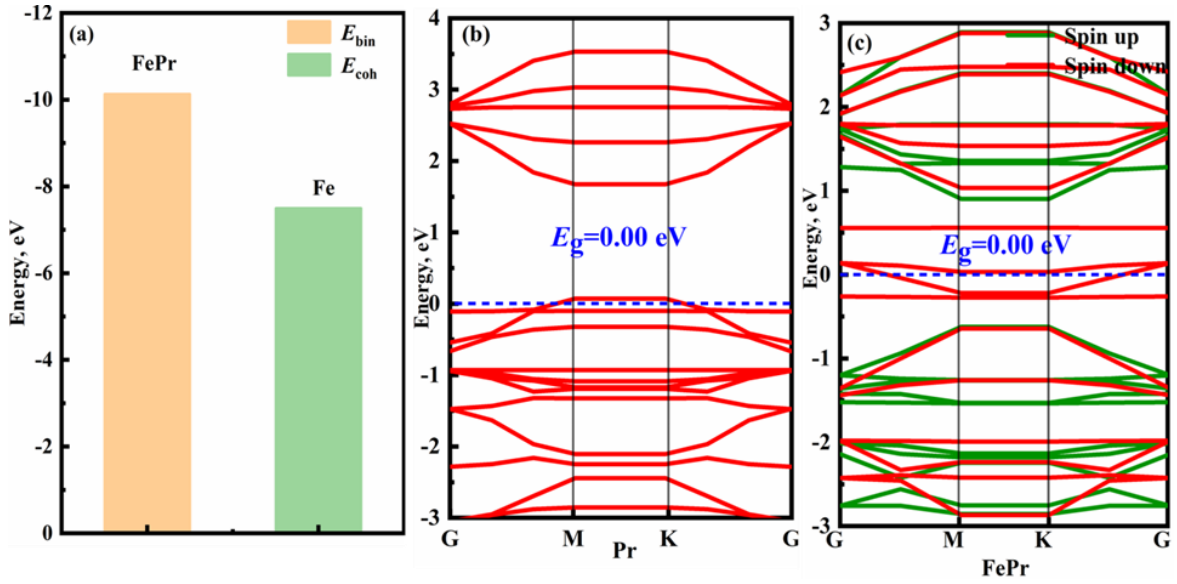

Figure 2. (a) Cohesive energy of Fe bulk (E_{coh}) and binding energy of FePr monolayer (E_{bin}), and band structure of the (b) Pr monolayer and (c) FePr monolayer.

The CDD analysis and the DOSs analysis for the FePr monolayer are depicted in Fig.3. As can be seen that all of the DOSs exhibit asymmetries, indicating that the FePr monolayer is a magnetic material. Fig. 3(a) displays the Fe atom loss of electrons, while all four N atoms gain electrons, leading to the formation of coordination bonds between the Fe atom and N atoms. Consequently, a strong Fe-N bonding is established, ensuring structural stability, while the unpaired bonds of C atoms are neutralized through passivation with H atoms. Fig.3 (b) shows the spin polarization states near the Fermi level are predominantly hybridized between the Fe-d and N-p orbitals. Moreover, The Fe-d-up displays significant hybridization with N4-p-up over the energy range of −3.26 eV to 2.03 eV, while the Fe-d-down orbital exhibits significant hybridization with N4-p-down orbitals within an energy range of −2.50 eV to 3.14 eV. In summary, the Fe-d orbital exhibits strong hybridization with the N4 of the Pr, resulting in a robust binding force between Fe and Pr monolayer.

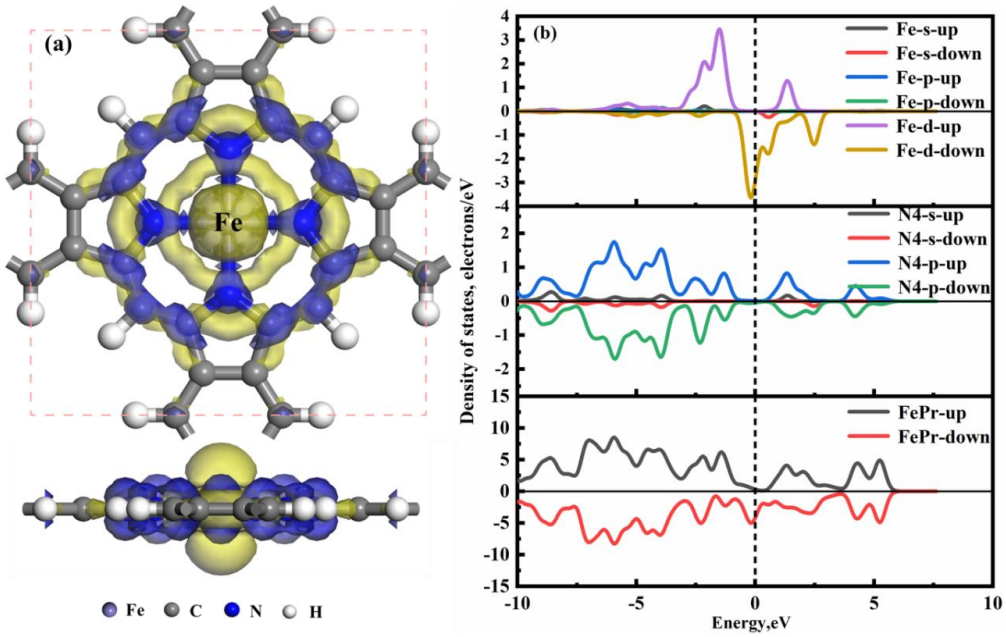

Figure 3. CDD and DOSs of (a, b) FePr monolayer, where N4 denotes the four closest neighboring N atoms to the Fe atom. The blue region indicates electron accumulation, while the yellow region indicates electron depletion, and the isosurface value of the CDD being ± 0.01 e/Å^3.

Preprints (www.preprints.org) | NOT PEER-REVIEWED | Posted: 13 June 2023 doi:10.20944/preprints202306.0912.v1

3.2. Adsorption of gases on Pr monolayer

The adsorption properties of SF_6 decomposition gases (H_2S, SO_2, SOF_2, SO_2F_2, and HF) on the Pr monolayer were first evaluated. One can be seen from Table 1 that all the adsorption energies are negative, meaning that the adsorption process is an exothermic reaction. It can be also observed that H_2S/SO_2 are preferentially adsorbed on the Pr monolayer with the S-end, while SOF_2 and SO_2F_2 gas molecules prefer to adsorb on the Pr monolayer with the O-end, and the HF molecules show a preference for adsorption on the Pr monolayer with F-end. Among the tested molecules, the lowest adsorption energy on the Pr monolayer belongs to the SO_2 molecule, followed by SOF_2, HF, SO_2F_2 and H_2S. The adsorption of SO_2 displays favorable strength, with adsorption energies of −0.69 eV. These findings indicate that the intrinsic Pr monolayer exhibits a moderate affinity towards SO_2. However, the intrinsic Pr monolayer exhibits poor sensitivity towards SO_2 due to its limited changes in E_g and M, as indicated in Table 1. By contrast, the Pr monolayer exhibits a low affinity towards H_2S, SOF_2, SO_2F_2 and HF molecules, indicating its poor capture capacity for these four gases. Therefore, the intrinsic Pr nanosheet is not a suitable sensing material for H_2S, SOF_2, SO_2F_2 and HF molecules.

Table 1. The adsorption energy (E_{ads}), the electron transfer (Q_T), adsorption height (H), band gap before and after adsorption (E_g' and E_g), and magnetic moment before and after adsorption (M' and M) of the optimal adsorption systems.

	Gases	Adsorption style	E_{ads}/eV	Q_T/e	H/Å	$E_g'(E_g)$/eV	$M'(M)/\mu_B$
Pr	H_2S	S-end	−0.14	0.063	2.466	0.000 (0.000)	0.000 (0.000)
	SO_2	S-end	−0.69	−0.130	2.161	0.000 (0.000)	0.000 (0.000)
	SOF_2	O-end	−0.18	0.006	2.861	0.000 (0.000)	0.000 (0.000)
	SO_2F_2	O-end	−0.12	−0.001	2.328	0.000 (0.000)	0.000 (0.000)
	HF	F-end	−0.17	0.086	2.533	0.000 (0.000)	0.000 (0.000)

Preprints (www.preprints.org) | NOT PEER-REVIEWED | Posted: 13 June 2023 doi:10.20944/preprints202306.0912.v1

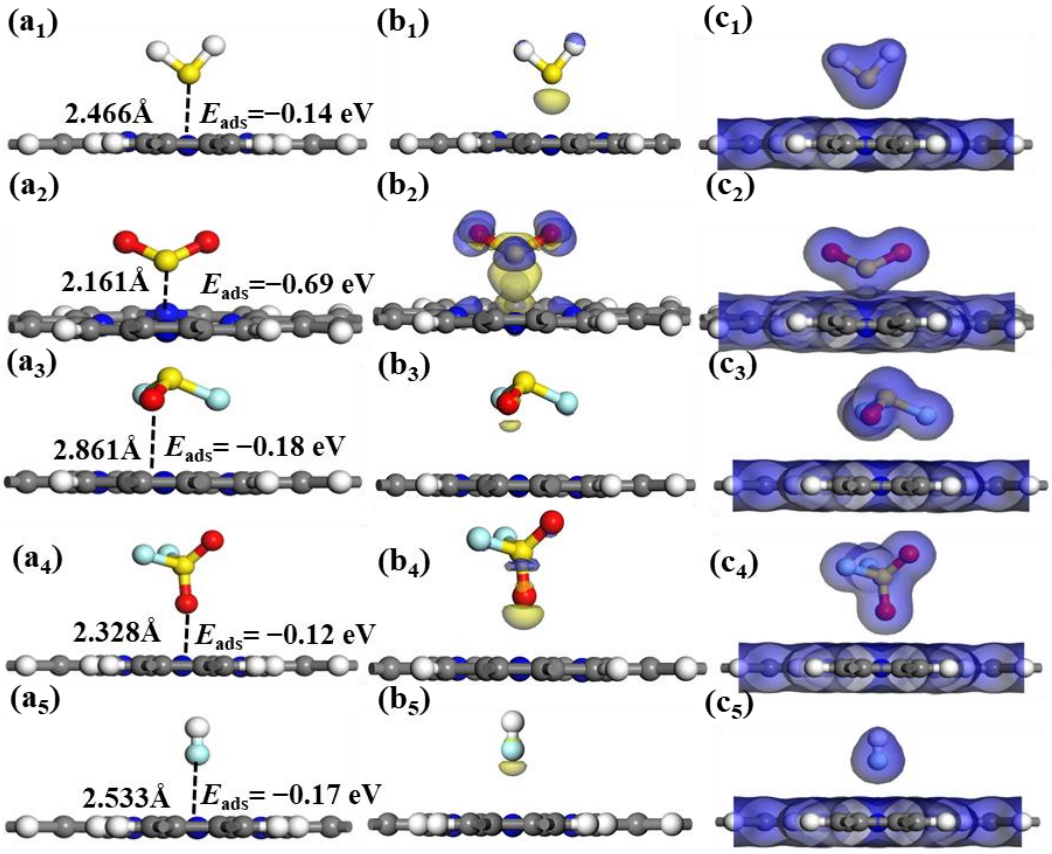

Figure 4. The stable adsorption configurations, CDD, and EDD of (a_1-c_1) H_2S, (a_2-c_2) SO_2, (a_3-c_3) SOF_2, (a_4-d_4) SO_2F_2 and （a_5-c_5）HF adsorbed on Pr monolayer. The blue region indicates electron accumulation, while the yellow region indicates electron depletion, the isosurface for CDD being ± 0.01 e/Å^3 and the isosurface for EDD being 0.2 e/Å^3.

The optimal adsorption systems, CDD and EDD for the five toxic gases adsorbed by intrinsic Pr monolayer are presented in Fig. 4. The preferential adsorption of SO_2, H_2S, SOF_2, SO_2F_2 and HF gas molecules is the cavity of the Pr monolayer, as presented in Fig.4 (a_1−a_5). According to Fig. 4 (b_1−b_5), it can be observed that the SO_2 and SO_2F_2 molecules undergo electron gain, while the other three molecules experience varying degrees of electron loss. Furthermore, the EDD analysis indicates a significant overlap in electron density distribution between SO_2 molecules and Pr monolayer. However, H_2S, SOF_2, SO_2F_2 and HF exhibit only minimal electron sharing with the Pr substrate, as illustrated in Fig. 4 (c_1-c_5). This also indicates that the Pr monolayer exhibits a greater interaction strength with SO_2 compared to the other four gases. To further determine the microscopic interactions of gas molecules and Pr monolayer, the corresponding DOSs for the Pr monolayer following gas adsorption are depicted in Fig. 5 (a-e). For SO_2, there are more resonance peaks observed in the Pr monolayer compared to the other four gases within energy ranging from −5.0 eV ~ 5.0 eV. Thus, the adsorption strength of SO_2 is greater than that the H_2S, SOF_2, SO_2F_2, and HF, which is consistent with the results obtained for E_{ads}.

Preprints (www.preprints.org) | NOT PEER-REVIEWED | Posted: 13 June 2023 doi:10.20944/preprints202306.0912.v1

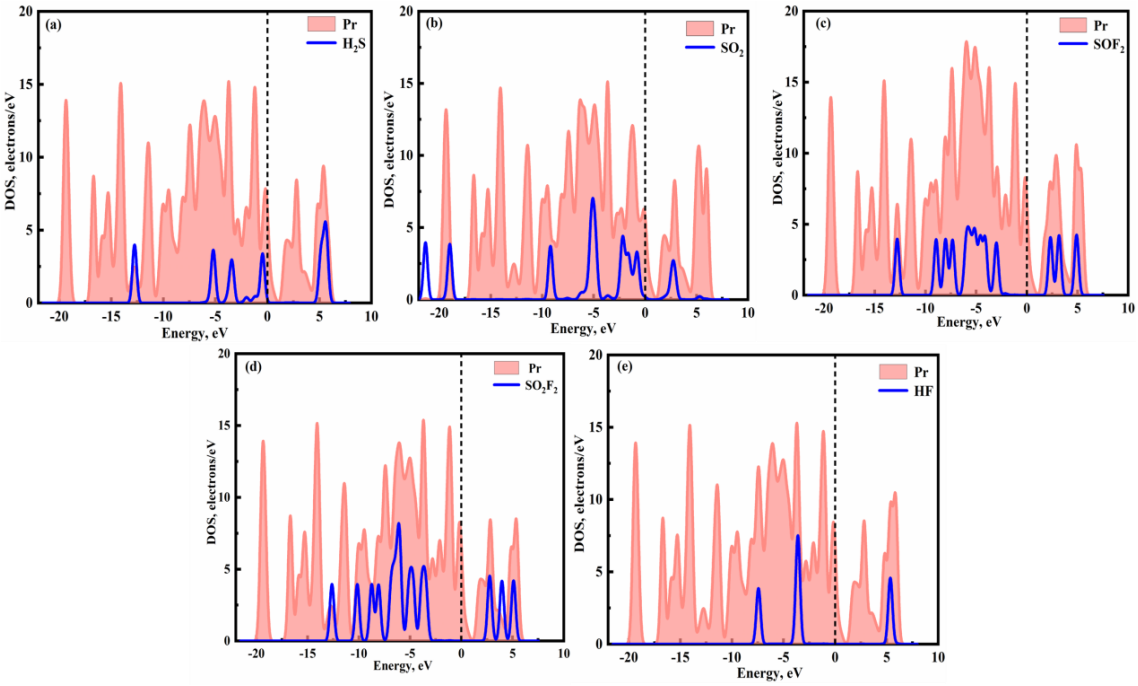

Figure 5. The DOSs of (a) H_2S, (b) SO_2, (c) SOF_2, (d) SO_2F_2, and (e) HF adsorbed on Pr.

3.3. Adsorption of gases on FePr monolayer

The adsorption of H_2S, SOF_2, SO_2, SO_2F_2, and HF gases on FePr monolayer was thoroughly investigated in this section, Table 2 presents the adsorption parameters and electronic performance of the studied gases. The calculated adsorption energies for H_2S, SO_2, SOF_2, SO_2F_2, and HF molecules are −0.42 eV, −0.86 eV, −0.78 eV, −0.33 eV and −0.33 eV, respectively. In terms of adsorption energies, the FePr monolayer exhibits a moderate adsorption capacity towards H_2S, SO_2 and SOF_2. However, its capture ability is weaker for SO_2F_2 and HF molecules. In addition, the FePr substrate receives approximately 0.350 e, 0.066 e, and 0.087 e from H_2S, SO_2 and SOF_2 gas molecules respectively. However, relatively small amounts of 0.027 e and 0.021 e were transferred to the FePr monolayer from SO_2F_2 and HF gases, respectively. This result implies that all the SF_6 decomposition components are electron acceptors. Moreover, a moderate Q_T leads to an appropriate adsorption capacity for H_2S, SOF_2 and SO_2, suggesting that the FePr monolayer has the potential as a gas capture material. Interestingly, the E_g and M of FePr appeared to change after the adsorption for H_2S, SO_2 and SOF_2, indicating excellent gas sensitivity of the FePr sheet towards these three gases.

Table 2. The adsorption energy (E_{ads}), the electron transfer (Q_T), adsorption height (H), band gap before and after adsorption (E_g' and E_g), and magnetic moment before and after adsorption (M' and M) of the optimal adsorption systems.

	Gases	Adsorption style	E_{ads}/eV	Q_T/e	H/Å	$E_g'(E_g)$/eV	$M'(M)/\mu_B$
FePr	H_2S	S-end	−0.42	0.350	2.168	1.013(0.000)	0.000(1.869)
	SO_2	S-end	−0.86	0.066	2.020	0.919(0.000)	0.000(1.869)
	SOF_2	S-end	−0.78	0.087	2.006	0.916(0.000)	0.000(1.869)
	SO_2F_2	O-end	−0.33	0.027	2.698	0.000(0.000)	1.879(1.869)
	HF	F-end	−0.33	0.021	2.655	0.000(0.000)	1.888(1.869)

Preprints (www.preprints.org) | NOT PEER-REVIEWED | Posted: 13 June 2023 doi:10.20944/preprints202306.0912.v1

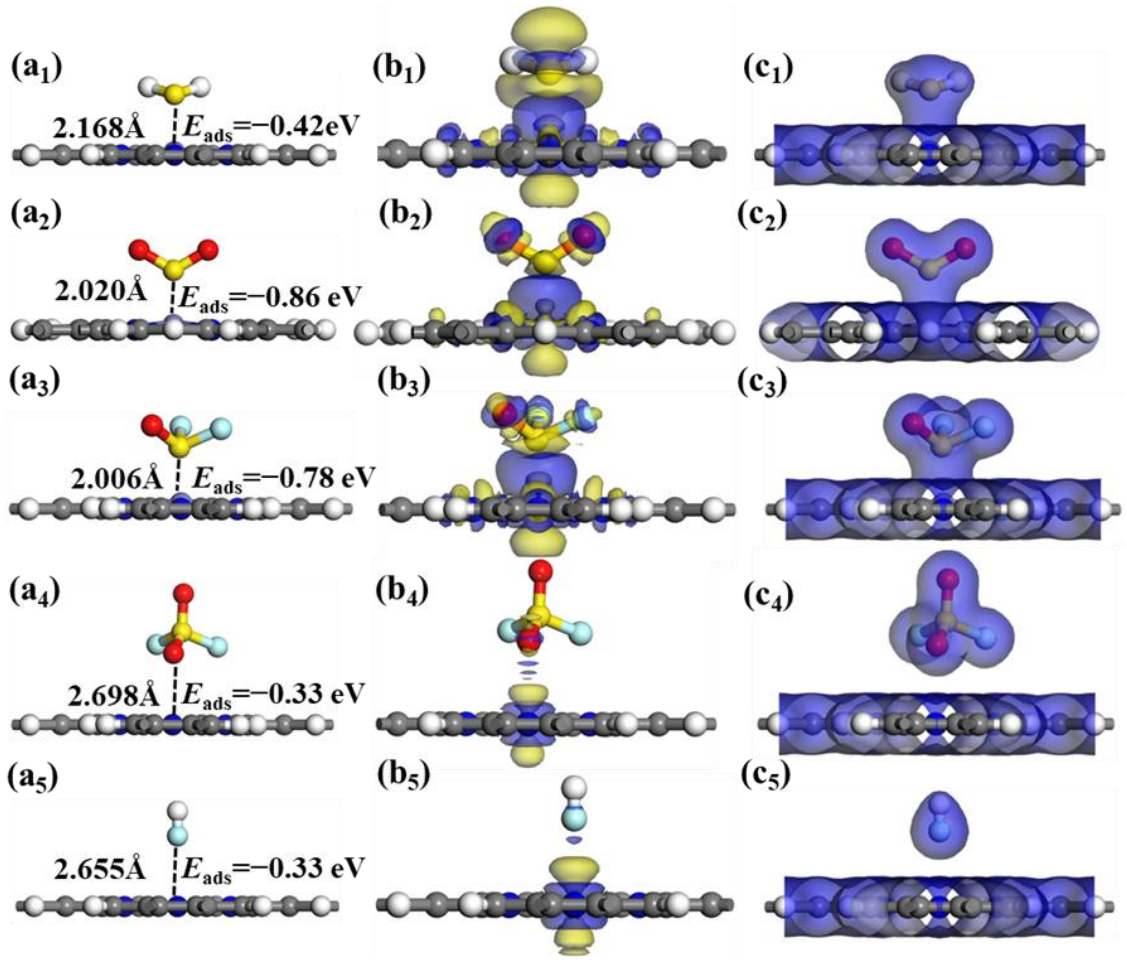

Figure 6. The CDD and EDD were calculated for the FePr monolayer. (a_1-c_1) H_2S, (a_2-c_2) SO_2, (a_3-c_3) SOF_2, (a_4-c_4) SO_2F_2 and (a_5-c_5) HF. The blue region indicates electron accumulation, while the yellow region indicates electron depletion, the isosurface for CDD being ± 0.01 e/Å^3 and the isosurface for EDD being 0.2 e/Å^3.

The optimal adsorption systems, CDD and EDD for the five toxic gases adsorbed by FePr monolayer are illustrated in Fig. 6. As shown in Fig. 6(a_1−a_5), the adsorption strength is SOF_2 > SO_2 > H_2S > SO_2F_2/HF. The high adsorption energies suggest chemisorption between the SOF_2, SO_2, and H_2S molecules and FePr substrate, while SO_2F_2 and HF molecules exhibit weak physisorption. From the CDD illustrated in Fig. 6 (b_1–b_3), it is apparent that a significant depletion of electrons occurs around the H_2S, SO_2 and SOF_2, while numerous electrons accumulate around the Fe atoms, this result suggests that the Fe atom received a significant amount of electrons from H_2S, SO_2, and SOF_2. The EDD diagrams depicted in Fig. 6(c_1-c_5) reveal a notable overlap of charge density among the H_2S@FePr, SO_2@FePr, and SOF_2@FePr adsorption systems, indicating a significant interaction between the gases and FePr monolayer. However, for the SO_2F_2@FePr and HF@FePr systems, no discernible overlap in electron density is observed. Consequently, the FePr monolayer demonstrates a higher affinity towards H_2S, SO_2 and SOF_2 molecules compared to SO_2F_2 and HF.

The DOSs and PDOSs for the FePr monolayer with adsorption of SF_6 decomposition components are presented in Fig. 7 and Fig. 8. When the HF and SO_2F_2 are adsorbed onto FePr monolayer (Fig. 8(d&e)), the limited number of occupied states near the Fermi level suggests a weak interaction between FePr monolayer and SO_2F_2/HF. Furthermore, as shown in Fig.8(d), the overlap between O-p and FeN4-d orbitals is only confined to the energy level of −10.39 eV, resulting in the feeble interaction of SO_2F_2 and FePr sheet. From Fig. 8(e), no resonance peaks are observed between F-p and FeN4-d orbitals. Therefore, the electronic properties of FePr are not significantly affected by HF molecule. Nevertheless, the H_2S, SO_2, and SOF_2 exert a significant influence on the electronic structure of the FePr monolayer. As shown in Fig.8(a), there are five distinct resonance

Preprints (www.preprints.org) | NOT PEER-REVIEWED | Posted: 13 June 2023 doi:10.20944/preprints202306.0912.v1

peaks at approximately −6.88 eV, −4.18 eV, −2.36 eV, −0.56 eV and 0.56 eV in the H_2S@FePr system. For SO_2 and SOF_2, the number of observed resonance peaks is greater for both gases when adsorbed on FePr monolayer compared to H_2S (Fig. 7(a-c)). This indicates that the adsorption strength of SOF_2 and SO_2 is greater than that of H_2S, which is consistent with the results of E_{ads}. In addition, as displayed in Fig. 8(b&c), there are significant orbital hybridizations between S-p and FeN4-p/d of SO_2/SOF_2 within the energy ranging from −10.0 to 7.5 eV. The significant orbital interactions lead to an appropriate adsorption capacity of SOF_2 and SO_2 molecules with the E_{ads} of −0.78 eV and −0.86 eV, which is advantageous for gas capture. Moreover, the FePr monolayer experiences a transition from a magnetic to a nonmagnetic state upon the adsorption of H_2S, SO_2, and SOF_2 molecules. While the magnetic properties of SO_2F_2 and HF molecules remain unchanged upon adsorption. The variation in the magnetic moment of the FePr monolayer is advantageous for the detection of diverse toxic gases.

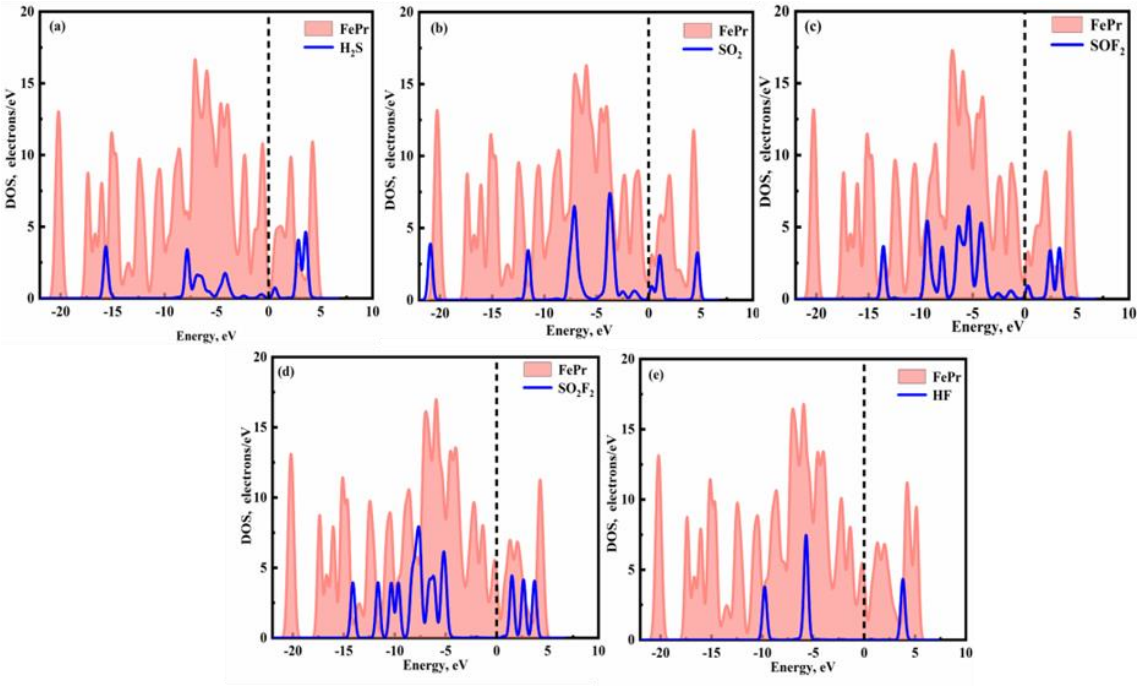

Figure 7. The DOSs of (a) H_2S, (b) SO_2, (c) SOF_2, (d) SO_2F_2, and (e) HF adsorbed FePr monolayer.

Preprints (www.preprints.org) | NOT PEER-REVIEWED | Posted: 13 June 2023 doi:10.20944/preprints202306.0912.v1

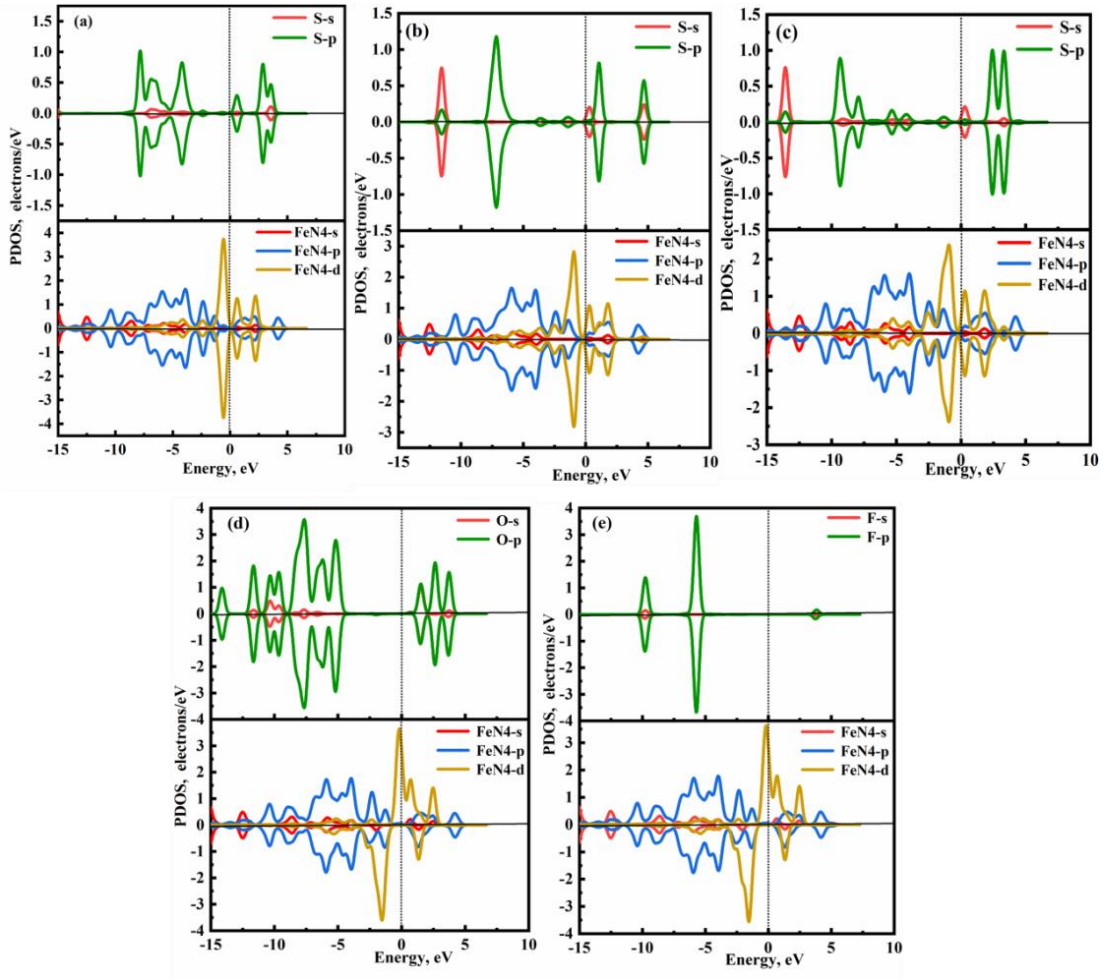

Figure 8. The PDOSs of adsorbed FePr monolayer with (a) H_2S, (b) SO_2, (c) SOF_2, (d)SO_2F_2, and (e)HF.

3.4. Sensing performance evaluation of FePr monolayer

In general, the conductivity (σ) of a material is closely related to the band gap (E_g), thus, the FePr nanosheet's sensitivity towards targeted gases can be assessed by the variations of conductivity, which can be defined as follows [44]:

$$\sigma \propto \exp(\frac{-E_g}{2K_B T}) \quad (4)$$

where E_g is bandgap, K_B is Boltzmann constant, and K is temperature.

Preprints (www.preprints.org) | NOT PEER-REVIEWED | Posted: 13 June 2023 doi:10.20944/preprints202306.0912.v1

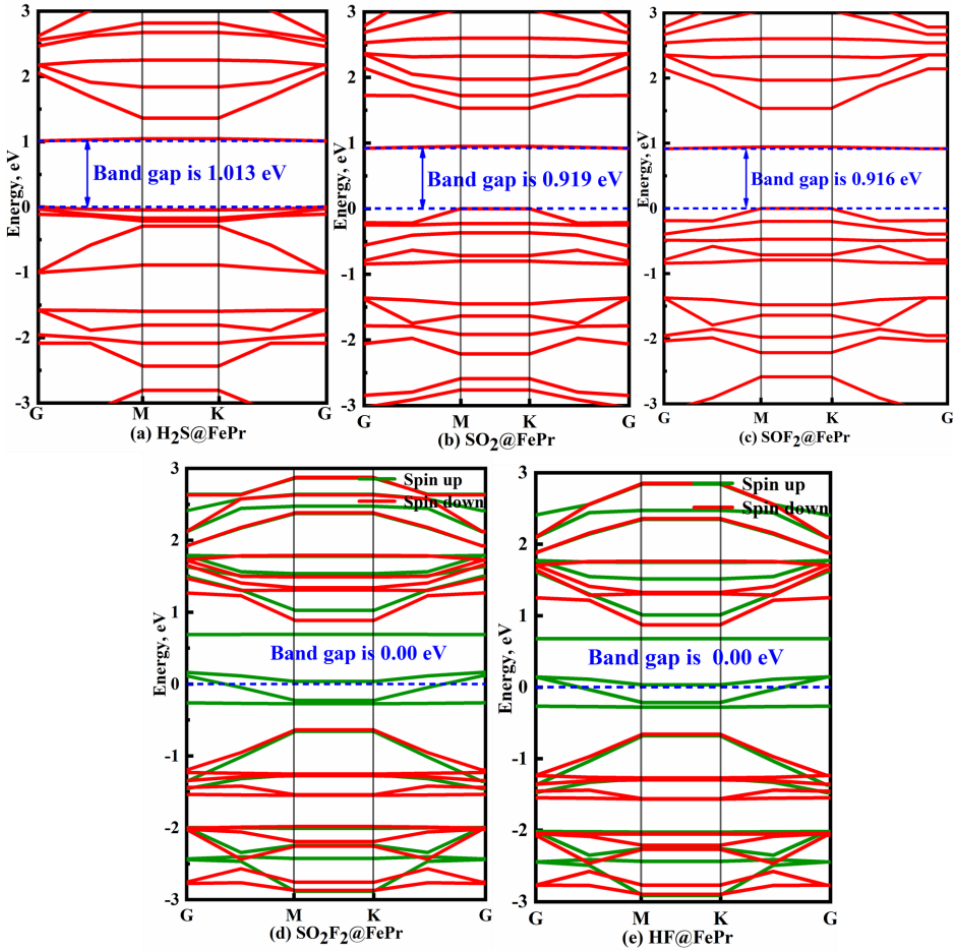

Figure 9. Band structure of adsorption systems can be defined as A@B, where A represents the gas molecule being adsorbed and B represents the substrate on which it is adsorbed.

The band structure of adsorption systems is illustrated in Fig. 9. Compared with the zero bandgaps of the FePr monolayer (Fig.2), the bandgap of FePr after H_2S, SO_2, and SOF_2 adsorption is changed to 1.013 eV, 0.919 eV and 0.916 eV, respectively. This suggests that the conducting property of intrinsic FePr is transformed into a semiconducting characteristic after gas adsorption. In other words, the FePr monolayer exhibits exceptional sensitivity towards H_2S, SO_2, and SO_2F_2. However, the adsorption of SO_2F_2 and HF molecules has a negligible effect on the E_g of the FePr monolayer, indicating its poor sensitivity towards these gases. Apart from the E_g, the variations in magnetic properties resulting from gas adsorption can be also served as an indicator for evaluating the sensitivity of a gas sensor. Most notably, the M of the FePr monolayer disappears after H_2S, SO_2, and SOF_2 adsorptions. Thus, the FePr monolayer demonstrates potential as a magnetic gas sensor for the detecting of H_2S, SO_2, and SOF_2 detection.

In addition, the sensitivity of the FePr monolayer can also be evaluated by measuring the change of work function (φ) before and after gas adsorption [45, 46], where φ is defined as:

$$\varphi = E_{\text{vaccum}} - E_{\text{fermi}} \quad (5)$$

The vacuum and Fermi levels of the FePr monolayer after gas adsorption is represented by E_{vaccum} and E_{fermi}, respectively.

The calculated φ of the FePr before and after gas adsorption are depicted in Fig.10. It can be observed that the work function of FePr undergoes significant changes upon the adsorption of SF_6 decomposition components. Compared to the FePr monolayer with the φ of 4.65 eV, the φ of the FePr monolayer increases to 5.25 eV and 5.22 eV after the SO_2 and SOF_2 adsorption, respectively. The increase in φ indicates the charge transfer from the FePr monolayer to gases, resulting in the formation of an interface dipole in the same direction [47, 48]. In contrast, the adsorption of H_2S, SO_2F_2, and HF on the intrinsic FePr monolayer leads to a reduction in the φ values to 4.57 eV, 4.40

Preprints (www.preprints.org) | NOT PEER-REVIEWED | Posted: 13 June 2023 doi:10.20944/preprints202306.0912.v1

eV, and 4.40 eV, respectively. Therefore, the FePr monolayer can also serve as a φ−type gas sensor for detecting H_2S, SO_2, SOF_2, SO_2F_2, and HF molecules.

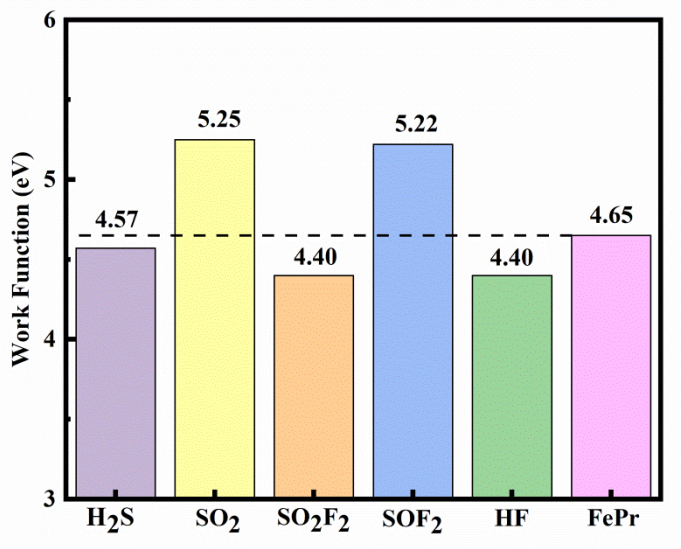

Figure 10. The work function of FePr monolayer before and after gas adsorption.

Additionally, the quantification of sensitivity (*Se*) can provide a more precise evaluation of gas sensor sensitivity [49], which is as follows:

$$Se=\left(\frac{1}{\sigma_{FePr/gas}}-\frac{1}{\sigma_{FePr}}\right)/\frac{1}{\sigma_{FePr}}=\exp\left[\left(E_{g\,FePr/gas}-E_{g\,FePr}\right)/2K_BT\right]-1 \quad (6)$$

where $\sigma_{FePr/gas}$ and σ_{FePr} indicate the conductivity of the FePr monolayer before and after gas adsorption, respectively.

Fig.11 shows the sensitivity of the FePr monolayer toward the SO_2, H_2S, and SOF_2 at the range temperatures of 298 to 498 K. The *Se* of the FePr monolayer towards SO_2, H_2S and SOF_2 at 298 K falls within the range of (2.07–13.7) $\times10^7$, which is significantly higher than that of SF_6 (approximately 10^3)[12]. In addition, the FePr monolayer displays the highest sensitivity to H_2S at each temperature, followed by SO_2 and SOF_2. The sensitivity of FePr towards SOF_2 was 2.07×10^7 at 298 K and 1.59×10^4 at 398 K. However, the sensitivity of FePr to H_2S/SO_2 exceeded that of SOF_2. With the increase in operating temperature, there was a slight decrease in the sensitivity of H_2S, SOF_2, and SO_2F_2. In conclusion, the FePr monolayer exhibits excellent sensing capabilities towards H_2S, SO_2, and SOF_2.

Preprints (www.preprints.org) | NOT PEER-REVIEWED | Posted: 13 June 2023 doi:10.20944/preprints202306.0912.v1

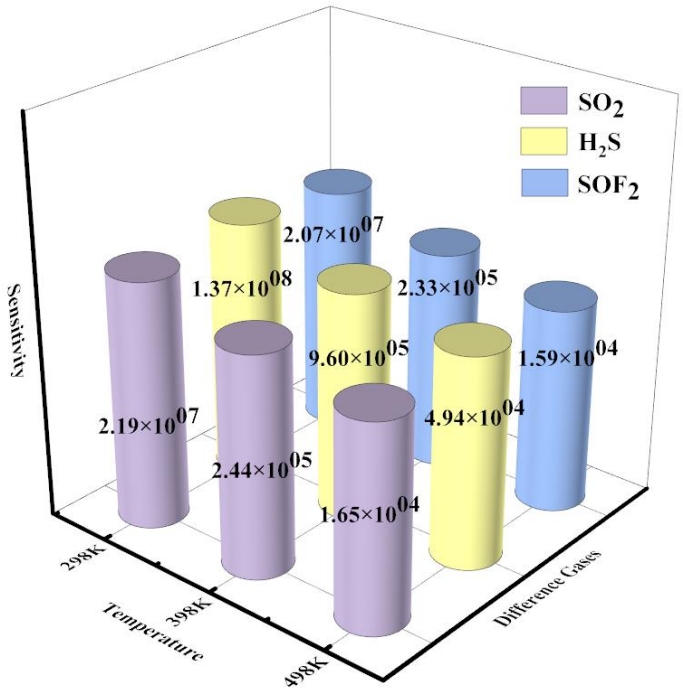

Figure 11. The sensitivity of the FePr monolayer toward the gases at the range temperatures of 298 K to 498 K.

Finally, the recovery time (τ) is strongly correlated with adsorption energy and can be determined by [50, 51]:

$$\tau = v_0^{-1} exp\left(\frac{-E_{ads}}{K_B T}\right) \quad (7)$$

where v_0, K_B, and T indicate the frequency factor, Boltzmann constant, and temperature, respectively.

Fig. 12 displays the τ of H_2S, SO_2, SOF_2, SO_2F_2, and HF molecules adsorption systems at the range temperatures of 298 K to 498 K. The FePr monolayer exhibits an extremely short recovery time for H_2S, SO_2, SOF_2, SO_2F_2, and HF molecules at working temperatures, indicating that these gases can be easily desorbed from the FePr monolayer. Interestingly, the τ of H_2S, SO_2, and SOF_2 is estimated to be 12.6 μs, 18.5 s, and 15.4 s at 298K, respectively. Therefore, the FePr is regarded as a promising, reusable gas sensor for detecting H_2S, SOF_2 and SO_2 due to its appropriate adsorption capacity and short desorption time.

Preprints (www.preprints.org) | NOT PEER-REVIEWED | Posted: 13 June 2023 doi:10.20944/preprints202306.0912.v1

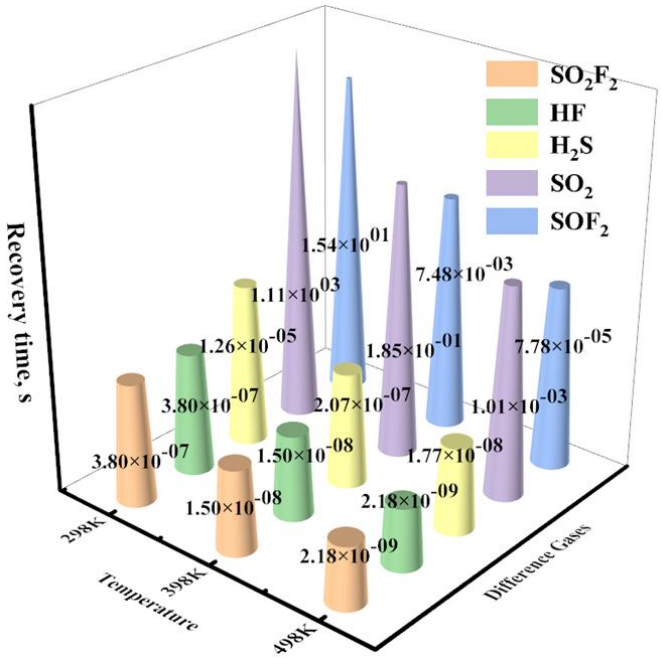

Figure 12. The recovery time of the different gases on FePr monolayer at the range temperatures of 298 K to 498 K.

4. Conclusions

In this paper, we investigated the adsorption characteristics of five primary SF_6 decomposition gases (H_2S, SO_2, SOF_2, SO_2F_2, HF) on the Pr and FePr monolayers using DFT computations. We also analyzed the electronic properties and sensing mechanisms of different adsorption systems. The main conclusions are succinctly outlined as follows:

(1) The thermodynamic stability of the FePr monolayer is attributed to the significant orbital hybridization between the Fe atom and the Pr monolayer surface.

(2) The FePr monolayer possesses a moderate capture capacity of $H_2S/SO_2/SOF_2$, while it exhibits weak adsorption ability of SO_2F_2 and HF gases due to the physical adsorption.

(3) The FePr monolayer has a higher affinity with H_2S, SO_2 and SOF_2 due to the robust orbital hybridizations between these gases and the FePr monolayer within an energy range of −10.0 to 7.5 eV.

(4) Due to its appropriate adsorption strength, exquisite sensitivity, and short recovery time, the FePr monolayer shows great potential as a recyclable gas sensor for detecting H_2S, SOF_2 and SO_2 detection.

Author Contributions: Conceptualization, Z. N.; methodology, E. D; visualization, X. H.; software, H. X.; validation, Q. C.; investigation, X. H.; Formal analysis, R. X.; data curation, E. D.; writing – original draft, X. H. and E. D.; writing - review & editing, Z. N. and H. X.; project administration, Z. N.; Funding acquisition, Z. N. All authors have read and agreed to the published version of the manuscript.

Funding: This work was supported by the National Natural Science Foundation of China (Grant No. 51904137), Special Basic Cooperative Research Programs of Yunnan Provincial Undergraduate Universities' Association (Grant No. 202101BA070001-032), Basic Research Project of Yunnan Province (202201AT070017), Scientific Research Funds of Yunnan Education Department (2023Y0901 and 2023Y0895), and Science and Technology Project of Yunnan Precious Metals Lab (No.YPML-2022050230). The authors also thank the High-Level Talent Plans for Young Top-notch Talents of Yunnan Province (Grant No. YNWR-QNBJ-2020-017) and High-Level Talent Special Support Plans for Young Talents of Kunming City (Grant No. C201905002).

Institutional Review Board Statement: Not applicable.

Informed Consent Statement: Not applicable.

Data Availability Statement: The data presented in this study is contained within the article.

Conflicts of Interest: The authors declare no conflict of interest.

Sample Availability: Not applicable.

Acknowledgments: We thank the editor and the reviewers for their useful help for improving this paper, along with the Scientific Innovation Team of Kunming University for helpful discussions on topics related to this work.

References

1. Kim, S.; Nagorny, P., Electrochemical Synthesis of Glycosyl Fluorides Using Sulfur(VI) Hexafluoride as the Fluorinating Agent. *Org Lett* **2022,** 24, (12), 2294-2298.
2. Hou, W.; Mi, H.; Peng, R.; Peng, S.; Zeng, W.; Zhou, Q., First-Principle Insight into Ga-Doped MoS_2 for Sensing SO_2, SOF_2 and SO_2F_2. *Nanomaterials (Basel)* **2021,** 11, (2).
3. Nagarajan, V.; Chandiramouli, R., SF_6 and SOF_2 interaction studies on novel Tricycle Red Phosphorene sheets based on first-principles studies. *Chemical Physics Letters* **2022,** 800, 139674.
4. Paul, T. A.; Porus, M.; Galletti, B.; Kramer, A., SF_6 concentration sensor for gas-insulated electrical switchgear. *Sensors and Actuators A: Physical* **2014,** 206, 51-56.
5. Xu, L.; Gui, Y.; Li, W.; Li, Q.; Chen, X., Gas-sensing properties of Ptn-doped WSe_2 to SF_6 decomposition products. *Journal of Industrial and Engineering Chemistry* **2021,** 97, 452-459.
6. Kim, K. H.; Ingole, P. G.; Kim, J. H.; Lee, H. K., Experimental investigation and simulation of hollow fiber membrane process for SF_6 recovery from GIS. *Polymers for Advanced Technologies* **2013,** 24, (11), 997-1004.
7. Liu, D.; Gui, Y.; Ji, C.; Tang, C.; Zhou, Q.; Li, J.; Zhang, X., Adsorption of SF_6 decomposition components over Pd (1 1 1): A density functional theory study. *Applied Surface Science* **2019,** 465, 172-179.
8. Li, Z.; Jia, L.; Chen, J.; Cui, X.; Zeng, W.; Zhou, Q., Ag-modified hexagonal GaN monolayer as an innovative gas detector toward SF_6 decomposed species: Insights from the first-principles computations. *Applied Surface Science* **2022,** 589, 153000.
9. Liao, Y.; Zhou, Q.; Peng, R.; Zeng, W., Adsorption properties of InP_3 monolayer toward SF_6 decomposed gases: A DFT study. *Physica E: Low-dimensional Systems and Nanostructures* **2021,** 130, 114689.
10. Wang, D.; Yang, A.; Lan, T.; Fan, C.; Pan, J.; Liu, Z.; Chu, J.; Yuan, H.; Wang, X.; Rong, M.; Koratkar, N., Tellurene based chemical sensor. *Journal of Materials Chemistry A* **2019,** 7, (46), 26326-26333.
11. Deng, P.; Cheng, L.; Jiang, P.; Zeng, Z.; Li, A.; Liao, C., Sensing performance of CdPc monolayer toward the SF_6 decomposition gases: A DFT study. *Chemical Physics Letters* **2022,** 806, 140030.
12. Nie, Z.; Wang, C.; Xue, R.; Xie, G.; Xiong, H., Two-dimensional FePc and MnPc monolayers as promising materials for SF_6 decomposition gases detection: Insights from DFT calculations. *Applied Surface Science* **2023,** 608, 155119.
13. Ma, S.; Li, D.; Rao, X.; Xia, X.; Su, Y.; Lu, Y., Pd-doped h-BN monolayer: a promising gas scavenger for SF_6 insulation devices. *Adsorption* **2020,** 26, (4), 619-626.
14. Zhang, H.; Ma, Y.; Xiong, H.; Deng, G.; Yang, L.; Nie, Z., Highly sensitive and selective sensing-performance of 2D Co-decorated phthalocyanine toward NH_3, SO_2, H_2S and CO molecules. *Surfaces and Interfaces* **2023,** 36, 102641.
15. Hou, W.; Liu, Y.; Zeng, W.; Zhou, Q., Theoretical screening into Ag-Embedded HfS_2 monolayers as gas sensor for detecting SF_6 decomposition gases. *Journal of Materials Research and Technology* **2022,** 18, 1991-2000.
16. Chen, D.; Zhang, X.; Tang, J.; Cui, H.; Pi, S.; Cui, Z., Adsorption of SF_6 Decomposed Products over ZnO($10\bar{1}0$): Effects of O and Zn Vacancies. *ACS Omega* **2018,** 3, (12), 18739-18752.
17. Faye, O.; Eduok, U.; Szpunar, J. A.; Beye, A. C., Two-dimensional carbon nitride (C_3N) nanosheets as promising materials for H_2S and NH_3 elimination: A computational approach. *Physica E: Low-dimensional Systems and Nanostructures* **2020,** 117, 113794.
18. Xiao-Hong, L.; Shan-Shan, L.; Yong-Liang, Y.; Rui-Zhou, Z., Adsorption of NH_3 onto vacancy-defected Ti_2CO_2 monolayer by first-principles calculations. *Applied Surface Science* **2020,** 504, 144325.
19. Ding, C.; Hu, X.; Feng, L.; Fernando, G., Study on the Adsorption Characteristics of Mo-Doped Graphene on the Decomposition Products of SF_6 Substitute Gas Based on First-Principle Calculations. *Advances in Condensed Matter Physics* **2022,** 2022, 1-9.

20. Cui, H.; Zhang, X.; Li, Y.; Chen, D.; Zhang, Y., First-principles insight into Ni-doped InN monolayer as a noxious gases scavenger. *Applied Surface Science* **2019,** 494, 859-866.
21. Hu, F.-F.; Tang, H.-Y.; Tan, C.-J.; Ye, H.-Y.; Chen, X.-P.; Zhang, G.-Q., Nitrogen Dioxide Gas Sensor Based on Monolayer SnS: A First-Principle Study. *IEEE Electron Device Letters* **2017,** 38, (7), 983-986.
22. Guo, Y.; Zhang, Y.; Wu, W.; Liu, Y.; Zhou, Z., Transition metal (Pd, Pt, Ag, Au) decorated InN monolayer and their adsorption properties towards NO_2: Density functional theory study. *Applied Surface Science* **2018,** 455, 106-114.
23. Yamamoto, A.; Mizuno, Y.; Teramura, K.; Hosokawa, S.; Shishido, T.; Tanaka, T., Visible-light-assisted selective catalytic reduction of NO with NH_3 on porphyrin derivative-modified TiO_2 photocatalysts. *Catalysis Science & Technology* **2015,** 5, (1), 556-561.
24. Ge, R.; Li, X.; Kang, S.-Z.; Qin, L.; Li, G., Highly efficient graphene oxide/porphyrin photocatalysts for hydrogen evolution and the interfacial electron transfer. *Applied Catalysis B: Environmental* **2016,** 187, 67-74.
25. Chen, D.; Wang, K.; Hong, W.; Zong, R.; Yao, W.; Zhu, Y., Visible light photoactivity enhancement via CuTCPP hybridized g-C_3N_4 nanocomposite. *Applied Catalysis B: Environmental* **2015,** 166-167, 366-373.
26. Abel, M.; Clair, S.; Ourdjini, O.; Mossoyan, M.; Porte, L., Single layer of polymeric Fe-phthalocyanine: an organometallic sheet on metal and thin insulating film. *J Am Chem Soc* **2011,** 133, (5), 1203-5.
27. Kim, J. H.; Lee, S. H.; Lee, J. S.; Lee, M.; Park, C. B., Zn-containing porphyrin as a biomimetic light-harvesting molecule for biocatalyzed artificial photosynthesis. *Chem Commun (Camb)* **2011,** 47, (37), 10227-9.
28. Wang, X.-Y.; Li, Y.-Q.; Zhu, S.-Y.; He, Q.-W.; Tang, D.-S.; Wang, X.-C., The adsorption characteristics of CO, NO and NO_2 on two dimensional metalloporphyrin porous nanosheets: A first-principles study. *Applied Surface Science* **2022,** 582, 152469.
29. Luo, G.; Wang, Y.; Li, Y., Two-dimensional iron-porphyrin sheet as a promising catalyst for oxygen reduction reaction: a computational study. *Sci Bull (Beijing)* **2017,** 62, (19), 1337-1343.
30. Yu, H.-X.; Mu, H.-M.; Zhu, D.-R.; Zhang, Y.; Wang, X.-C.; Xiao-An Zhang, S., DFT study on the oxygen titanium porphyrin as sustainable cyclic catalyst for water splitting. *International Journal of Hydrogen Energy* **2019,** 44, (36), 19920-19928.
31. Delley, B., From molecules to solids with the $DMol^3$ approach. *The Journal of Chemical Physics* **2000,** 113, (18), 7756-7764.
32. Zeng, J.; Xu, L.; Luo, X.; Chen, T.; Tang, S.-H.; Huang, X.; Wang, L.-L., Z-scheme systems of ASi_2N_4 (A = Mo or W) for photocatalytic water splitting and nanogenerators. *Tungsten* **2021,** 4, (1), 52-59.
33. Grimme, S., Semiempirical GGA-type density functional constructed with a long-range dispersion correction. *J Comput Chem* **2006,** 27, (15), 1787-99.
34. Delley, B., Hardness conserving semilocal pseudopotentials. *Physical Review B* **2002,** 66, (15).
35. Vozzi, C.; Negro, M.; Calegari, F.; Sansone, G.; Nisoli, M.; De Silvestri, S.; Stagira, S., Generalized molecular orbital tomography. *Nature Physics* **2011,** 7, (10), 822-826.
36. Monkhorst, H. J.; Pack, J. D., Special points for Brillouin-zone integrations. *Physical Review B* **1976,** 13, (12), 5188-5192.
37. Xiong, H.-h.; Zhang, H.-n.; Dong, J.-h., Adhesion strength and stability of TiB_2/TiC interface in composite coatings by first principles calculation. *Computational Materials Science* **2017,** 127, 244-250.
38. Liu, Y.; Zhou, Q.; Wang, J.; Zeng, W., Cr doped MN (M = In, Ga) monolayer: A promising candidate to detect and scavenge SF6 decomposition components. *Sensors and Actuators A: Physical* **2021,** 330, 112854.
39. Yong, Y.; Cui, H.; Zhou, Q.; Su, X.; Kuang, Y.; Li, X., C_2N monolayer as NH_3 and NO sensors: A DFT study. *Applied Surface Science* **2019,** 487, 488-495.
40. Gui, X.; Zhou, Q.; Peng, S.; Xu, L.; Zeng, W., Adsorption behavior of Rh-doped MoS_2 monolayer towards SO_2, SOF_2, $SO2F_2$ based on DFT study. *Physica E: Low-dimensional Systems and Nanostructures* **2020,** 122, 114224.
41. Xu, L.; Zeng, J.; Li, Q.; Luo, X.; Chen, T.; Liu, J.; Wang, L.-L., Multifunctional silicene/CeO_2 heterojunctions: Desirable electronic material and promising water-splitting photocatalyst. *Chinese Chemical Letters* **2022,** 33, (8), 3947-3950.
42. Sun, Q.; Dai, Y.; Ma, Y.; Li, X.; Wei, W.; Huang, B., Two-dimensional metalloporphyrin monolayers with intriguing electronic and spintronic properties. *Journal of Materials Chemistry C* **2015,** 3, (26), 6901-6907.
43. Xiong, H.; Liu, B.; Zhang, H.; Qin, J., Theoretical insight into two-dimensional M-Pc monolayer as an excellent material for formaldehyde and phosgene sensing. *Applied Surface Science* **2021,** 543, 148805.
44. Esrafili, M. D.; Arjomandi Rad, F., Carbon-doped boron nitride nanosheets as highly sensitive materials for detection of toxic NO and NO_2 gases: A DFT study. *Vacuum* **2019,** 166, 127-134.

 doi:10.20944/preprints202306.0912.v1

45. Roondhe, B.; Jha, P. K.; Ahuja, R., Haeckelite boron nitride as nano sensor for the detection of hazardous methyl mercury. *Applied Surface Science* **2020,** 506, 144860.
46. Peng, S.; Cho, K.; Qi, P.; Dai, H., Ab initio study of CNT NO_2 gas sensor. *Chemical Physics Letters* **2004,** 387, (4-6), 271-276.
47. Yu, Y.-X., A dispersion-corrected DFT study on adsorption of battery active materials anthraquinone and its derivatives on monolayer graphene and h-BN. *J. Mater. Chem. A* **2014,** 2, (23), 8910-8917.
48. Kistanov, A. A.; Cai, Y.; Zhou, K.; Dmitriev, S. V.; Zhang, Y.-W., The role of H_2O and O_2 molecules and phosphorus vacancies in the structure instability of phosphorene. *2D Materials* **2016,** 4, (1), 015010.
49. Xia, S.-Y.; Tao, L.-Q.; Jiang, T.; Sun, H.; Li, J., Rh-doped h-BN monolayer as a high sensitivity SF_6 decomposed gases sensor: A DFT study. *Applied Surface Science* **2021,** 536, 147965.
50. Xu, Z.; Shi, Z.; Wang, M.; Song, R.; Zhang, X.; Liu, G.; Qiao, G., Gas sensing properties of defective tellurene on the nitrogen oxides: A first-principles study. *Sensors and Actuators A: Physical* **2021,** 328, 112766.
51. Liu, Y.; Gui, Y.; Chen, X., Adsorption and sensing performances of ZnO-g-C_3N_4 monolayer toward SF_6 decomposition products. *Physica E: Low-dimensional Systems and Nanostructures* **2021,** 134, 114909.